J|A|C|S ARTICLES

Published on Web 10/26/2010

Quantitative Analysis of Protein Backbone Dynamics in Microcrystalline Ubiquitin by Solid-State NMR Spectroscopy

Paul Schanda,* Beat H. Meier, and Matthias Ernst*

ETH Zürich, Physical Chemistry, Wolfgang-Pauli-Strasse 10, 8093 Zürich, Switzerland

Received January 27, 2010; E-mail: pasa@nmr.phys.chem.ethz.ch; maer@ethz.ch

Abstract: Characterization of protein dynamics by solid-state NMR spectroscopy requires robust and accurate measurement protocols, which are not yet fully developed. In this study, we investigate the backbone dynamics of microcrystalline ubiquitin using different approaches. A rotational-echo double-resonance type (REDOR-type) methodology allows one to accurately measure $^{1}H-^{15}N$ order parameters in highly deuterated samples. We show that the systematic errors in the REDOR experiment are as low as 1% or even less, giving access to accurate data for the amplitudes of backbone mobility. Combining such dipolar-coupling-derived order parameters with autocorrelated and cross-correlated ^{15}N relaxation rates, we are able to quantitate amplitudes and correlation times of backbone dynamics on picosecond and nanosecond time scales in a residue-resolved manner. While the mobility on picosecond time scales appears to have rather uniform amplitude throughout the protein, we unambiguously identify and quantitate nanosecond mobility with order parameters S^2 as low as 0.8 in some regions of the protein, where nanosecond dynamics has also been revealed in solution state. The methodology used here, a combination of accurate dipolar-coupling measurements and different relaxation parameters, yields details about dynamics on different time scales and can be applied to solid protein samples such as amyloid fibrils or membrane proteins.

Introduction

Conformational flexibility is a key prerequisite for function and stability of proteins. A comprehensive description of protein function, therefore, requires not only information about the static ground-state structure but also information about the thermally accessible conformational space, which can be obtained in the form of amplitudes and time scales of conformational fluctuations. NMR spectroscopy has proven a very successful tool to study protein dynamics in solution[1−3] because of its ability to provide residue-resolved insight into the dynamics over a wide range of time scales. Spectral resolution and sensitivity of solid-state NMR has recently reached a point that allows also structural studies of crystalline[4−8] and noncrystalline protein samples such as amyloid fibrils[9−13] or membrane proteins in a nativelike environment.[14,15] These achievements also form the basis for studying protein dynamics with residue resolution in solids[11,16−24] that complement and extend studies using single-site labeling approaches, as used for low-temperature measurements.[25,26] The absence of overall molecular tumbling in the solid state opens new possibilities for the study of dynamics.

(1) Palmer, A. *Chem. Rev.* **2004**, *104*, 3623–40.
(2) Ishima, R.; Torchia, D. *Nat. Struct. Biol.* **2000**, *7*, 740–3.
(3) Mittermaier, A.; Kay, L. *Science* **2006**, *312*, 224–8.
(4) Manolikas, T.; Herrmann, T.; Meier, B. *J. Am. Chem. Soc.* **2008**, *130*, 3959–66.
(5) Castellani, F.; van Rossum, B.; Diehl, A.; Schubert, M.; Rehbein, K.; Oschkinat, H. *Nature* **2002**, *420*, 98–102.
(6) Loquet, A.; Bardiaux, B.; Gardiennet, C.; Blanchet, C.; Baldus, M.; Nilges, M.; Malliavin, T.; Böckmann, A. *J. Am. Chem. Soc.* **2008**, *130*, 3579–89.
(7) Franks, W.; Wylie, B.; Schmidt, H.; Nieuwkoop, A.; Mayrhofer, R.; Shah, G.; Graesser, D.; Rienstra, C. *Proc. Natl. Acad. Sci. U.S.A.* **2008**, *105*, 4621–6.
(8) Zech, S.; Wand, A.; McDermott, A. *J. Am. Chem. Soc.* **2005**, *127*, 8618–26.
(9) Wasmer, C.; Lange, A.; Van Melckebeke, H.; Siemer, A.; Riek, R.; Meier, B. *Science* **2008**, *319*, 1523–6.
(10) Andronesi, O.; von Bergen, M.; Biernat, J.; Seidel, K.; Griesinger, C.; Mandelkow, E.; Baldus, M. *J. Am. Chem. Soc.* **2008**, *130*, 5922–8.
(11) Heise, H.; Hoyer, W.; Becker, S.; Andronesi, O.; Riedel, D.; Baldus, M. *Proc. Natl. Acad. Sci. U.S.A.* **2005**, *102*, 15871–6.
(12) Petkova, A.; Ishii, Y.; Balbach, J.; Antzutkin, O.; Leapman, R.; Delaglio, F.; Tycko, R. *Proc. Natl. Acad. Sci. U.S.A.* **2002**, *99*, 16742–7.
(13) Jaroniec, C.; MacPhee, C.; Bajaj, V.; McMahon, M.; Dobson, C.; Griffin, R. *Proc. Natl. Acad. Sci. U.S.A.* **2004**, *101*, 711–6.
(14) McDermott, A. *Annu. Rev. Biophys.* **2009**, *38*, 385–403.
(15) Lange, A.; Giller, K.; Hornig, S.; Martin-Eauclaire, M.; Pongs, O.; Becker, S.; Baldus, M. *Nature* **2006**, *440*, 959–62.
(16) Chevelkov, V.; Fink, U.; Reif, B. *J. Biomol. NMR* **2009**, *45*, 197–206.
(17) Giraud, N.; Blackledge, M.; Goldman, M.; Böckmann, A.; Lesage, A.; Penin, F.; Emsley, L. *J. Am. Chem. Soc.* **2005**, *127*, 18190–201.
(18) Yang, J.; Tasayco, M.; Polenova, T. *J. Am. Chem. Soc.* **2009**, *131*, 13690–702.
(19) Schneider, R.; Seidel, K.; Etzkorn, M.; Lange, A.; Becker, S.; Baldus, M. *J. Am. Chem. Soc.* **2010**, *132*, 223–33.
(20) Huster, D.; Xiao, L. S.; Hong, M. *Biochemistry* **2001**, *40*, 7662–74.
(21) Helmus, J.; Surewicz, K.; Surewicz, W.; Jaroniec, C. *J. Am. Chem. Soc.* **2010**, *132*, 2393–403.
(22) Lange, A.; Gattin, Z.; Van Melckebeke, H.; Wasmer, C.; Soragni, A.; van Gunsteren, W. F.; Meier, B. H. *ChemBioChem* **2009**, *10*, 1657–65.
(23) Ader, C.; Pongs, O.; Becker, S.; Baldus, M. *Biochim. Biophys. Acta* **2010**, *1798*, 286–90.
(24) Franks, W.; Zhou, D.; Wylie, B.; Money, B.; Graesser, D.; Frericks, H.; Sahota, G.; Rienstra, C. *J. Am. Chem. Soc.* **2005**, *127*, 12291–305.
(25) Vugmeyster, L.; Ostrovsky, D.; Ford, J. J.; Lipton, A. S. *J. Am. Chem. Soc.* **2010**, *132*, 4038–9.

First, the full range of time scales of internal motions is visible in solid-state NMR relaxation measurements in contrast to solution-state NMR relaxation measurements where all information about internal dynamics that are slower than the overall tumbling are masked. Dynamics on a nanosecond to microsecond time scale, which may involve significant structural rearrangements and can be of functional relevance, can, therefore, be characterized quantitatively in terms of amplitudes and time scales. On the basis of this realization, a recent study has undertaken a combined analysis of solid- and solution-state relaxation data, revealing the presence of nanosecond motion that is not detected in aqueous solution.[27] Second, anisotropic interactions such as dipolar couplings are not averaged to zero, and their magnitude can be measured. Of particular interest is the dipolar coupling between directly bonded nuclei, such as side-chain or backbone C−H or amide N−H dipolar couplings, for which the rigid-limit value can readily be calculated without any knowledge of the 3D structure from the almost constant bond length. The measurement of these one-bond dipolar couplings leads to a direct determination of order parameters, S, that characterize the amplitude of motions occurring on time scales up to the inverse of the coupling strength, i.e., typically up to microseconds.

Here we present a comprehensive study of the backbone dynamics of the protein ubiquitin over time scales from picoseconds to several microseconds. To obtain residue-resolved order parameters and time scales of backbone dynamics in the crystal, we use the combined information from ^{1}H−^{15}N dipolar couplings and ^{15}N relaxation data. In principle, time scales and amplitudes of dynamics could be retrieved from longitudinal NMR relaxation (R_1) or cross-correlated relaxation[28] data in the solid state measured at different field strengths. In practice, however, such data are generally not sufficient to obtain precise information about order parameters.[16,17] This is due to the functional form of the R_1 and cross-correlated relaxation rates in the solid state, exhibiting only a weak dependence on the magnetic field strength (vide infra and Figure S9 of the Supporting Information). The availability of an accurate value of the ^{1}H−^{15}N dipolar coupling is, therefore, a crucial part of such an analysis.

The measurement of ^{1}H−^{15}N dipolar couplings in MAS solid-state NMR to determine order parameters of dynamics faster than several microseconds requires that the MAS-averaged dipolar coupling be reintroduced by a recoupling sequence. Several different recoupling schemes have been used to quantitatively measure the motionally averaged dipolar coupling in proteins.[19,24,29−33] Such quantitative measurements are challenged by two main difficulties: (i) the effect of homonuclear and heteronuclear couplings to remote spins on the observed ^{1}H−^{15}N recoupling behavior and (ii) the unavoidable effect of radio frequency field (rf-field) inhomogeneity over the sample volume as well as rf miscalibration. Both factors lead to errors in the measured dipolar-coupling constants. The influence of couplings to remote spins can be addressed by the design of the pulse sequences. However, pulse sequences that suppress the effects of homonuclear couplings to remote spins, such as Lee−Goldburg CP[34,35] or symmetry-based R-type sequences[36] are sensitive to rf-field inhomogeneity, which makes their quantitative interpretation difficult.[33,37] Alternatively, deuteration can be used to remove a large majority of ^{1}H spins and, thereby, reduce the effects of homonuclear ^{1}H−^{1}H couplings and heteronuclear couplings to remote ^{1}H spins. Chevelkov et al. have recently used a sample that is fully deuterated at all nonsolvent-exchangeable sites and 90% deuterated at all exchangeable sites to quantify ^{1}H−^{15}N dipolar couplings in a crystalline sample of the SH3 protein domain. They used a phase-inverted CP experiment that is less sensitive to rf inhomogeneity than regular CP.[32] Because pulsed recoupling experiments in combination with phase cycling[38] can be made less dependent on rf inhomogeneity than sequences that apply rf irradiation continuously, we implemented a rotational-echo double-resonance (REDOR[39]) based experiment to measure the ^{1}H−^{15}N dipolar couplings in a highly deuterated protein sample. We show its robustness with respect to experimental imperfections and structure-dependent factors such as chemical-shift anisotropies and remote spins. In the REDOR experiment, systematic errors of order parameters are generally below about 1%, giving thus access to highly accurate values for the motional amplitudes. Combining information from dipolar couplings and relaxation measurements, we obtain residue-specific order parameters and time scales for backbone dynamics. Clear evidence for nanosecond motion is found in some regions of the protein, while picosecond dynamics appears to be relatively uniform throughout the protein.

Measurement Protocols

Accurate Measurement of ^{1}H−^{15}N Dipolar Couplings. For the measurement of ^{1}H−^{15}N dipolar couplings we apply the pulse sequence shown in Figure 1a, which is a proton-detected HSQC-type ^{1}H−^{15}N correlation experiment that exploits scalar-coupling-based coherence-transfer steps. A REDOR dephasing period of the ^{15}N coherences by recoupling of the ^{1}H−^{15}N dipolar coupling is added in the center of this sequence. The REDOR heteronuclear recoupling makes use of rotor-synchronized π pulses to prevent the averaging of the dipolar couplings by MAS. Since the one-bond ^{1}H−^{15}N dipolar coupling is comparable to the spinning frequency, a regular REDOR pulse sequence, which employs π pulses at integers and half-integers of the MAS period, leads to a rapid dephasing of coherences. Consequently, the sampling of this damped oscillation at integer values of the rotor period is relatively sparse on the steep initial portion of the dephasing (see Figure 1b, red curve). For limited sensitivity, this situation reduces the precision of the measured dipolar couplings, because sensitivity may not be sufficient to retrieve accurate information from the tail of the damped

(26) Lazo, N. D.; Hu, W.; Cross, T. A. *J. Magn. Reson., Ser. B* **1995**, *107*, 43–50.
(27) Chevelkov, V.; Zhuravleva, A. V.; Xue, Y.; Reif, B.; Skrynnikov, N. R. *J. Am. Chem. Soc.* **2007**, *129*, 12594–5.
(28) Chevelkov, V.; Faelber, K.; Schrey, A.; Rehbein, K.; Diehl, A.; Reif, B. *J. Am. Chem. Soc.* **2007**, *129*, 10195–200.
(29) Lorieau, J.; McDermott, A. *J. Am. Chem. Soc.* **2006**, *128*, 11505–12.
(30) Hong, M.; Yao, X.; Jakes, K.; Huster, D. *J. Phys. Chem. B* **2002**, *106*, 7355–64.
(31) Seidel, K.; Etzkorn, M.; Sonnenberg, L.; Griesinger, C.; Sebald, A.; Baldus, M. *J. Phys. Chem. A* **2005**, *109*, 2436–42.
(32) Chevelkov, V.; Fink, U.; Reif, B. *J. Am. Chem. Soc.* **2009**, *131*, 14018–22.
(33) Zhao, X.; Sudmeier, J.; Bachovchin, W.; Levitt, M. *J. Am. Chem. Soc.* **2001**, *123*, 11097–8.
(34) Lee, M.; Goldburg, W. *Phys. Rev.* **1965**, *140*, 1261–5.
(35) Hester, R.; Ackerman, J.; Cross, V.; Waugh, J. *Phys. Rev. Lett.* **1975**, *34*, 993–5.
(36) Zhao, X.; Eden, M.; Levitt, M. *Chem. Phys. Lett.* **2001**, *342*, 353–61.
(37) Lorieau, J.; McDermott, A. *Magn. Reson. Chem.* **2006**, *44*, 334–47.
(38) Gullion, T.; Baker, D.; Conradi, M. *J. Magn. Reson.* **1990**, *89*, 479–84.
(39) Gullion, T.; Schaefer, J. *J. Magn. Reson.* **1989**, *81*, 196–200.

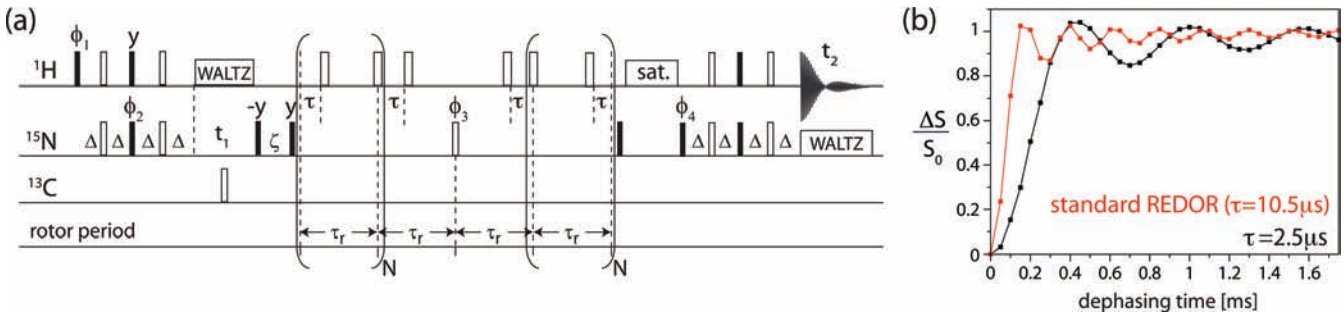

Figure 1. (a) Pulse sequence used for the measurement ^{1}H−^{15}N dipolar-coupling constants in highly deuterated proteins. Filled and open rectangles denote 90 and 180° pulses, respectively. The pulse and receiver phases were set to $\varphi_1 = 2(x), 2(-x)$; $\varphi_2 = x$; $\varphi_3 = x, -x$; $\varphi_4 = y, -y$; and $\varphi_{rec} = x, 2(-x), x$. Quadrature detection in t_1 was achieved by alternating φ_2 according to the states-TPPI scheme. The phases of the 180° ^{1}H pulses during the REDOR pulse train were incremented (decremented) according to the XY-16 scheme[38] in the block preceding (following) the central ^{15}N pulse. The phases of all other pulses were set to x. The delay Δ was set to 2.4 ms and the z-filter delay ζ was set to 20 ms. WALTZ decoupling of ^{1}H and ^{15}N was applied at an rf-field amplitude of $\nu_1 = 3$ and 2.5 kHz, respectively. The solvent saturation pulse was applied for 5 ms at a field strength of $\nu_1 = 10$ kHz. The effect of varying the delay τ is shown in panel b for a value of $\delta_D = 20.5$ kHz. A regular REDOR experiment, applying the π pulses at integer and half-integer rotor periods (red curve) is compared to a version where π pulses are shifted with $\tau = 2.5$ μs.

REDOR oscillations. To improve this situation, it is important to scale the effective dipolar oscillation frequency in order to better sample the REDOR curve. This can be achieved by applying the π pulses not at integer and half-integer multiples of the rotor period but by shifting one of the two sets of π pulses, as indicated in Figure 1.[40] The recoupled dipolar interaction is then reduced in a manner depending on the delay between the π pulses, τ, and on the pulse length. For the limiting case of inifinitely short pulses this scaling has been discussed.[40] A comparison of the dephasing in regular REDOR and the shifted REDOR variant is shown in Figure 1b.

REDOR curves are normalized, universal signatures of the strength of the dipolar coupling and depend only on the anisotropy of the dipolar coupling,

$$\delta_D = -2\frac{\mu_0 \gamma_H \gamma_N \hbar}{4\pi r_{NH}^3} \quad (1)$$

where γ_H and γ_N denote the gyromagnetic ratio of ^{1}H and ^{15}N, r_{NH} is the effective bond length, μ_0 is the magnetic permeability of free space, and $\hbar$ is Planck's constant. Fitting of REDOR curves, therefore, relies on a single fit parameter, which is the quantity of interest, without any dependence on the absolute signal intensity. This is in contrast to other methods for measuring dipolar couplings, such as CP variants,[29,32] TMREV,[41] or R-sequences,[33] where the signal intensity is also a fit parameter.

The experimentally measured magnitude of the dipolar interaction, δ_D^{expt}, gives direct access to the order parameter

$$\langle S \rangle = \delta_D^{expt}/\delta_D^{rigid} \quad (2)$$

where the rigid-limit value, δ_D^{rigid}, is calculated from the H−N bond length, which has a value of approximately 1.015[42] to 1.02 Å.[43] These variations are within the confidence interval of the determination.[42] Note that eq 2 assumes that the motion is axially symmetric and would require modification if anisotropic motions are present.

To verify the robustness of the shifted REDOR method for measuring ^{1}H−^{15}N dipolar couplings and to identify potential sources of systematic errors, we have investigated the influence of experimental parameters and the details of the spin system on the observed REDOR curves using numerical simulations. As shown in Figures S1−S4 of the Supporting Information, the method is very robust with respect to all realistic sources of imperfection. The influence of isotropic chemical-shift offsets and variations in ^{1}H or ^{15}N chemical-shielding anisotropy (CSA) tensors on the REDOR curve is barely detectable in simulations and can safely be neglected. Deviations introduced by the presence of additional ^{1}H spins as well as pulse miscalibration or rf-field inhomogeneities are detectable but small. The systematic errors induced by a realistic combination of all these factors are in all cases below about 1%. They are, therefore, generally within the random error of the experiments. These numerical simulations underline the robustness of the pulse sequence shown in Figure 1 for accurate quantification of ^{1}H−^{15}N dipolar couplings.

^{15}N Relaxation-Rate Constants. Amide ^{15}N relaxation-rate constants are sensitive to time scales and amplitudes of dynamics that involve reorientation of the ^{1}H−^{15}N bond vector and the ^{15}N CSA tensor. They can, therefore, complement the information about motional amplitudes obtained from dipolar-coupling measurements and add information about the time scale of the motion. Within the Redfield theory of nuclear spin relaxation, the longitudinal ^{15}N autorelaxation-rate constant (R_1) depends on the spectral-density functions J_m that describe the motion of the amide moiety[44,45]

$$R_1 = \frac{1}{10}\left(\frac{\mu_0}{4\pi}\frac{\gamma_N \gamma_H \hbar}{r_{NH}^3}\right)^2 \{J_0(\omega_H - \omega_N) + 3J_1(\omega_N) + 6J_2(\omega_H + \omega_N)\} + \frac{2}{15}(\omega_N(\Delta\sigma))^2 J_1(\omega_N) \quad (3)$$

Here $\Delta\sigma = \sigma_{zz} - \sigma_{xx}$ is the difference of the parallel and perpendicular components of the ^{15}N CSA tensor which is assumed to be axially symmetric. In the solid state, systematic errors in ^{15}N longitudinal relaxation-rate constants may arise

(40) Gullion, T.; Schaefer, J. *Adv. Magn. Reson.* **1989**, *13*, 57–83.
(41) Hohwy, M.; Jaroniec, C.; Reif, B.; Rienstra, C.; Griffin, R. *J. Am. Chem. Soc.* **2000**, *122*, 3218–9.
(42) Yao, L.; Vögeli, B.; Ying, J.; Bax, A. *J. Am. Chem. Soc.* **2008**, *130*, 16518–20.
(43) Bernado, P.; Blackledge, M. *J. Am. Chem. Soc.* **2004**, *126*, 4907–20.
(44) Abragam, A. *The Principles of Nuclear Magnetism*; Clarendon Press: Oxford, U.K., 1961.
(45) Torchia, D.; Szabo, A. *J. Magn. Reson.* **1982**, *49*, 107–21.

as a consequence of proton-driven ^{15}N spin diffusion,[46] which is best suppressed by employing fast MAS in combination with a high degree of sample deuteration,[47] as used in our study.

Additional information can be obtained from cross-correlated relaxation between the ^{1}H−^{15}N dipolar-coupling and the ^{15}N CSA interactions.[48−50] Measurement of this relaxation parameter requires high resolution in the ^{15}N dimension without ^{1}H decoupling, which can be achieved in deuterated samples. The cross-correlated relaxation-rate constant is given by

$$\eta = \frac{1}{15}\left(\frac{\mu_0}{4\pi}\frac{\gamma_N\gamma_H\hbar}{r_{NH}^{\ 3}}\right)(\omega_N(\Delta\sigma))\, P_2(\cos\theta)\{4J_0(0) + 3J_1(\omega_N)\} \quad (4)$$

where θ is the angle between the N−H bond and the symmetry axis of the ^{15}N CSA tensor. To calculate the relaxation-rate constants of eqs 3 and 4, the functional form of the spectral-density functions $J_m(\omega)$ is required. Analytical expressions for the correlation functions and, therefore, also for the spectral-density functions are available for a number of simple models, such as the diffusion-in-a-cone or jump models.[45] The data can also be interpreted using the so-called model-free approach,[51,52] where the motion is characterized by a set of generalized order parameters and correlation times. In liquids, the simplest case includes two motions, the overall tumbling with an order parameter of 0 and the internal motion with a correlation time shorter than the one for the overall tumbling. The model-free formalism allows the inclusion of additional motional modes in an approach that is referred to as "extended model-free approach".[53] It allows identifying and quantifying internal motional processes on more than one time scale. It should be noted that the model-free approach assumes that the $J_m(\omega)$ have the same form for all m, which is indeed the case in liquids but not always fulfilled in solids. As a further complication, a multiexponential decay is expected in solid-state NMR relaxation because $J_m(\omega)$ depends on the orientation of a crystallite with respect to a rotor-fixed coordinate system. Therefore, a powder averaging and an averaging over the MAS rotation must be performed.

Despite this inherent multiexponential nature of relaxation in solids, Torchia and Szabo[45] have proposed to evaluate the experimental data in terms of a monoexponential decay where the rate constants are MAS and powder averaged. Following this work, Emsley and co-workers have more recently proposed an "explicit average sum" approach which consists of explicitly calculating the multiexponential decay and fitting the initial slope using a monoexponential approximation.[17]

We have compared the relaxation-rate constants obtained from the more rigorous explicit-average-sum diffusion-in-a-cone treatment with the ones obtained from a model-free approach. Following the expressions given by Lipari and Szabo,[51,52] which correlate the parameters of model-free and diffusion-in-a-cone approaches, we have calculated the longitudinal relaxation-rate constants as a function of the order parameter S^2 and the correlation time τ_e for the two approaches (Figure 2). These simulations show that for high order parameters, ($S^2 > 0.7$) as found for backbone amide sites and for correlation times in the picosecond to nanosecond range, the model-free approach results in very similar relaxation-rate constants as a more rigorous diffusion-in-a-cone treatment. The deviations in the relevant area of the parameter space are below a few percent and usually far below the experimental errors (Figure 2d). On the basis of these simulations, we conclude that, for the regime investigated here and the relaxation-rate constants found experimentally (see below), the model-free analysis of experimental data yields the same results as an analysis using the orientation-dependent diffusion-in-a-cone model. Skrynnikov has come to similar conclusions for the cross-correlated relaxation rate constant η.[50] Using the model-free approach rather than diffusion-in-a-cone has the additional benefit that the treatment can be extended to multiple motions on different time scales, which is not easily possible in the framework of the diffusion-in-a-cone model. The latter would require a model of a bond vector diffusing in a cone that diffuses in another cone, for which, to our knowledge, no analytical expressions are available.

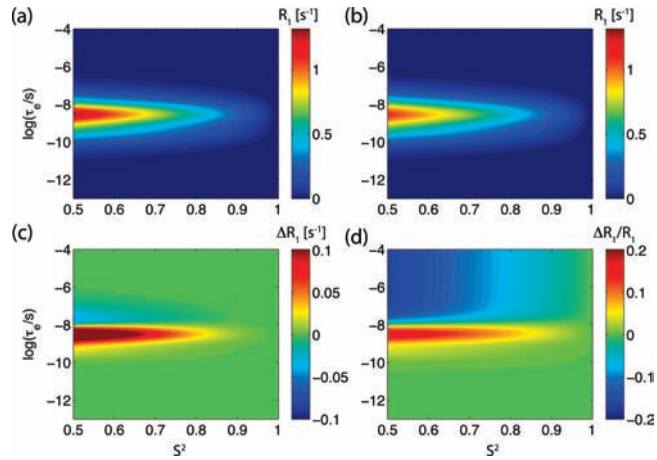

Figure 2. Comparison of dipolar-coupling-induced R_1 relaxation-rate constants for (a) the explicit-average-sum treatment of the diffusion-in-a-cone model[17] fitting the initial 15 s of the decay monoexponentially and (b) the model-free approach using an NH distance of 1.02 Å and a proton Larmor frequency of 500 MHz. Panel c shows the absolute difference between a and b, and d, the relative difference of a−b and a.

The simulated ^{15}N R_1 relaxation-rate constants within the framework of the model-free approach shown in Figures 2b and S9a,b of the Supporting Information reveal that the most efficient R_1 relaxation is expected when the time scale of the motion is on the order of the Larmor frequencies, i.e., when the correlation time τ is on a time scale of about 10^{-8}−10^{-9} s. Simulated cross-correlated relaxation-rate constants η, shown in Figure S9c,d of the Supporting Information, are expected for motions occurring on longer time scales due to the importance of the $J(0)$ contributions. Experimentally measurable cross-correlated relaxation rates of above a few s^{-1} require a motional correlation time longer than about a nanosecond. The cross-correlated relaxation is, thus, a very sensitive and direct means to probe nanosecond motion.[50] Both relaxation-rate constants discussed here, R_1 and η, are dependent on the magnetic field strength, and this field dependence can be used to increase the precision of the motional parameters. The field dependence of a single relaxation-rate constant is, however, generally not sufficient to

(46) Giraud, N.; Blackledge, M.; Böckmann, A.; Emsley, L. *J. Magn. Reson.* **2007**, *184*, 51–61.
(47) Chevelkov, V.; Diehl, A.; Reif, B. *J. Chem. Phys.* **2008**, *128*, 052316.
(48) Chevelkov, V.; Reif, B. *Concepts Magn. Reson., Part A* **2008**, *32A*, 143–56.
(49) Chevelkov, V.; Diehl, A.; Reif, B. *Magn. Reson. Chem.* **2007**, *45*, S156–S60.
(50) Skrynnikov, N. *Magn. Reson. Chem.* **2007**, *45*, S161–S73.
(51) Lipari, G.; Szabo, A. *J. Am. Chem. Soc.* **1982**, *104*, 4546–59.
(52) Lipari, G.; Szabo, A. *J. Am. Chem. Soc.* **1982**, *104*, 4559–70.
(53) Clore, G.; Szabo, A.; Bax, A.; Kay, L.; Driscoll, P.; Gronenborn, A. *J. Am. Chem. Soc.* **1990**, *112*, 4989–91.

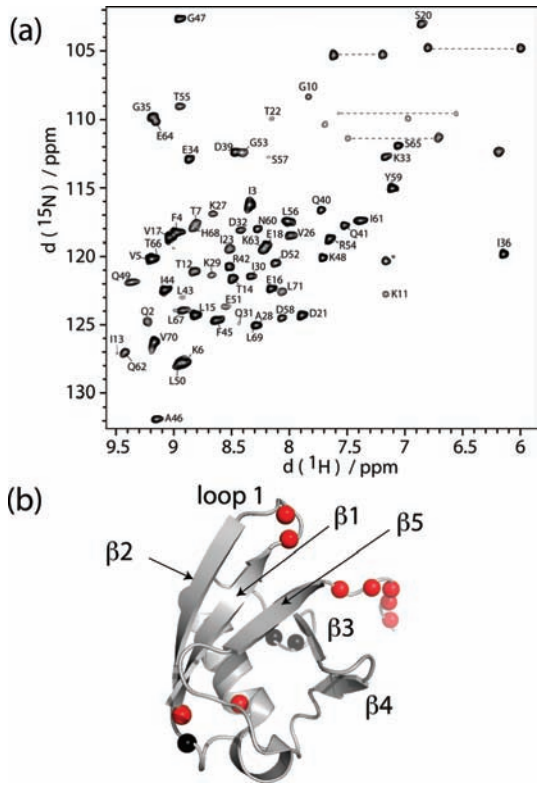

Figure 3. (a) ^{1}H, ^{15}N correlation spectrum obtained for the highly deuterated ubiquitin sample used in this study, measured at 301 K at a magnetic field strength of 19.96 T and a MAS frequency of 45 kHz. Residue-specific resonance assignment is indicated. A cartoon representation of the backbone structure is shown in b. Amide sites for which no ^{1}H, ^{15}N cross-peaks are observable (M1, L8, T9, E24, N25, R72, L73, R74, G75, and G76) are depicted as red spheres, and proline residues are shown as black spheres. Note that residue M1 is not observable in solution either, because of fast solvent exchange. The cross-peak of I13 is weak in CP- and *J*-coupling-based spectra.

determine motional parameters accurately,[16,17] and the availability of dipolar order parameters is a key requirement for a successful characterization of backbone dynamics.

In the following, we use ^{1}H$-^{15}$N dipolar order parameters in combination with up to five relaxation-rate constants (R_1 and η) per amide ^{15}N site to obtain information about the amplitudes and time scales of backbone motion. The data are fit to a two-time-scale model-free approach. The spectral-density function is assumed to be of the form

$$J(\omega) = (1 - S_f^2)\frac{\tau_f}{1 + (\omega\tau_f)^2} + S_f^2(1 - S_s^2)\frac{\tau_s}{1 + (\omega\tau_s)^2} \quad (5)$$

with two correlation times τ_f and τ_s and the corresponding two order parameters for a fast and a slow motion expressed by S_f^2 (τ_f) and S_s^2 (τ_s).

Results and Discussion

Proton-Detected High-Resolution Spectra and Assignments. We have used a perdeuterated sample of ubiquitin in microcrystalline form, protonated at 30% of the exchangeable hydrogen sites, to record scalar-coupling-based ^{1}H$-^{15}$N and ^{1}H$-^{15}$N$-^{13}$C correlation spectra. Figure 3a shows a ^{1}H-detected ^{1}H$-^{15}$N HSQC spectrum. A total of 63 out of the 76 residues in ubiquitin could be observed. From a set of scalar-coupling-based HNCA, HNCO, and HN(CO)CA experiments,[54] all amide cross-peaks in the ^{1}H$-^{15}$N spectrum were assigned site specifically (assignment reported in Table S1 of the Supporting Information). Missing correlation peaks can be an indicator of line broadening induced by dynamics in the corresponding regions and are investigated more closely. Besides the proline residues that do not bear an amide ^{1}H, and the N-terminal residue, the nonobservable amide sites (shown in Figure 3b) are located in the loop connecting the first two β-strands (L8 and T9), in the α-helix (E24 and N25) and in the C-terminus (residues 72−76). It is noteworthy that the residues located in the first loop as well as the C-terminal residues are also unobservable in dipolar-coupling-based solid-state NMR experiments.[55,56] While this observation could be attributed to a strong motion-induced reduction of the dipolar couplings, which makes dipolar-coupling-based transfer steps in such experiments inefficient, the fact that these correlation peaks are also invisible in scalar-coupling-based experiments points to different mechanisms.

A number of dynamic scenarios could explain the broadening of some peaks beyond detection. One possibility is the presence of conformational-exchange processes on microsecond-to-millisecond time scales, which involve states with different chemical shifts. This situation would lead to an apparent increase in the transverse relaxation-rate constant, also referred to as "exchange contribution to R_2".[57] Alternatively, Redfield relaxation through dipolar and CSA mechanisms could also be the origin of the line broadening, assuming that the amplitude is relatively large or the time scale is long. In this case, one expects that ^{15}N CSA, ^{1}H$-^{15}$N dipolar cross-correlated relaxation is efficient, and one might be able to recover some of the signals using TROSY-type spectroscopy, depending on the exact nature of the motion in terms of amplitude and time scale.[28] Such a scenario has been observed in solid-state NMR, where TROSY-type techniques resulted in significant enhancement and sharpening of signals broadened almost beyond detection in experiments using decoupling.[28,58] As a third possible scenario, static disorder or exchange between different states on time scales much slower than the chemical-shift difference of the involved states could also be an explanation for the disappearance of the cross-peaks. In this scenario, the signal would be distributed over several states with different frequencies (or a continuum of states), which can result in very broad lines below the detection limit.

To further investigate the origin of the disappearance of cross-peaks in microcrystalline ubiquitin, we have measured the transverse decay-rate constant, R_2', at high magic angle spinning frequency (57 kHz; see Figure S13 of the Supporting Information). Although in the solid state this rate constant not only depends on incoherent relaxation processes but also contains contributions from coherent broadening mechanisms, which prohibits a rigorous analysis in terms of dynamics, it is interesting to note that the observable residues in the first loop (T7, G10, and K11) show significantly faster transverse decays than other residues in the protein. This suggests the presence of dynamics in this region that leads to line broadening of the

(54) Linser, R.; Fink, U.; Reif, B. *J. Magn. Reson.* **2008**, *193*, 89–93.
(55) Igumenova, T.; McDermott, A.; Zilm, K.; Martin, R.; Paulson, E.; Wand, A. *J. Am. Chem. Soc.* **2004**, *126*, 6720–7.
(56) Schubert, M.; Manolikas, T.; Rogowski, M.; Meier, B. *J. Biomol. NMR* **2006**, *35*, 167–73.
(57) Cavanagh, J.; Fairbrother, W.; Palmer, A.; Skelton, N. *Protein NMR Spectroscopy: Principles and Practice*; Academic Press: San Diego, CA, 1996.
(58) Linser, R.; Fink, U.; Reif, B. *J. Am. Chem. Soc.* **2010**, *132*, 8891–3.

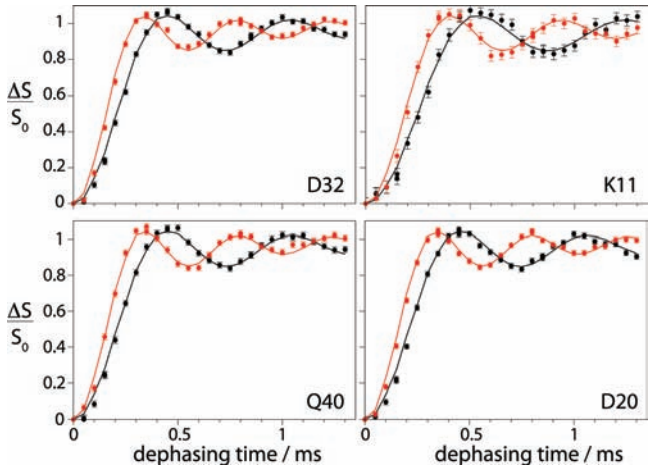

Figure 4. Representative experimental examples of REDOR curves observed for four different amide moieties in ubiquitin. Shown are the results from two different experiments that differ in the size of the delay τ (black, $\tau = 2.5$ μs; red, $\tau = 3$ μs), resulting in a different scaling factor of the oscillation frequency. Solid lines show best fits to the experimental data using only one fit parameter for simultaneous fitting of both data sets. Multiple points for a given dephasing time indicate duplicate measurements.

unobservable residues L8 and T9 either through chemical-shift modulation or enhanced Redfield-type relaxation. The observation of efficient ^{15}N CSA, ^{1}H$-^{15}$N dipolar cross-correlated relaxation in observable residues in this loop region (vide infra) suggests that the latter scenario is at the origin of the line broadening. Residue I23, preceding the unobservable residues E24 and N25, also displays enhanced transverse dephasing. However, it does not show significantly increased cross-correlated relaxation as compared to other secondary structure elements. In solution state it has been found that this N-terminal part of the α-helix displays conformational exchange dynamics on a microsecond time scale in solution, as probed by $T_{1\rho}$ experiments[59] and multiple-quantum experiments.[60,61] It is tempting to speculate that such conformational exchange dynamics are preserved in the solid state, providing an explanation for the invisibility of residues E24 and N25 in HSQC spectra. The reasons why the C-terminal residues are unobservable remains unclear, because there is no clear evidence of enhanced transverse relaxation or cross-correlated relaxation in the residues preceding this region.

Finally, we considered the possibility that missing cross-peaks can be recovered by the use of TROSY spectroscopy[28] or experiments performed at different temperatures. However, neither a TROSY experiment[62] (recorded at 14.09 T, 28 °C) nor scalar-coupling-based 2D experiments at lower (5 °C) or higher temperature (35 °C) revealed any additional cross-peaks.

Dipolar Order Parameters. For the measurement of ^{1}H$-^{15}$N dipolar couplings in ubiquitin, we have used the pulse sequence of Figure 1 at a MAS frequency of 40 kHz. Experimental examples of site-specific REDOR curves are shown in Figure 4. Two sets of experiments that differ in the length of the delay τ and, thus, result in a different scaling of the dipolar oscillations are shown. The REDOR data from three experimental series with different delays τ and two different pulse durations were fit jointly with the anisotropy of the ^{1}H$-^{15}$N dipolar coupling tensor, δ_D, as the only fit parameter. The fitted values of δ_D are shown in Figure 5 as a function of the residue position. In principle, H−N bond elongation through intramolecular hydrogen bonding might have a strong effect on these couplings, which would be manifest as reduced dipolar couplings for hydrogen-bonded sites. To test whether this is the case, or whether dipolar couplings are rather dominated by local dynamics, we have plotted the obtained dipolar couplings δ_D as a function of the $^{1}H^{N}$ chemical shift of the involved amide site (Figure S5), as the latter is known to correlate with the magnitude of hydrogen bond scalar couplings.[63] We find that the (weak) correlation is opposite to the one expected if N−H bond elongation through hydrogen bonding was a dominant factor and that overall the largest values of δ_D are observed for hydrogen-bonded amide sites. Therefore, similar to previous studies,[29,32] we conclude that reduced dipolar couplings are not due to H−N bond length elongation induced by hydrogen bonding but reflect indeed motional averaging.

Motional order parameters S are relatively uniform throughout the molecule in the range 0.8−0.9. If the amide bond-vector motion is expressed by the picture of a vector that freely diffuses within a cone, the average cone-opening half-angle extracted from the observed order parameters[51] is approximately 25° (Figure 5a). Notable exceptions with larger mobility are residues G10 and K11, I36, D52, and G53, which are all located in loop regions. An interesting pattern is observed within β-strand 2 (Figure 5b), where hydrogen-bonded residues with side chains pointing into the hydrophobic core (L15, V17) have significantly higher order parameters than the neighboring non-hydrogen-bonded residues with side chains pointing outward (T14, E16). This trend is also reflected in the relaxation-rate constants (vide infra). This alternating pattern also confirms that hydrogen-bond-induced elongation of H−N bonds is not an explanation for residue-to-residue differences of the dipolar coupling: if hydrogen bonding was a determining factor for δ_D, the alternating pattern would be in the opposite sense. The influence of side chain packing and hydrogen bonding on backbone dynamics has been suggested before to explain alternations of high-/low-order parameters derived from RDCs in solution in this region of ubiquitin (β-strand 2) and also in β-strand 4[64] (although some of the features reported initially for β-strand 2 were not reproduced in a more complete later analysis[65]) as well as in studies of backbone dynamics in solution from relaxation data.[66,67] Likewise, an alternating pattern of order parameters has been identified in protein G in the solution state using residual dipolar couplings.[68] In this case, the exposure of side chains has also been identified as the potential origin of the alternation.

^{15}N Relaxation Experiments. ^{1}H-detected ^{1}H$-^{15}$N correlation experiments were used to measure ^{15}N R_1 and ^{15}N CSA, ^{1}H, ^{15}N dipole cross-correlated relaxation-rate constants. The pulse sequences, shown in Figure S6 of the Supporting Information, are implemented using scalar-coupling-based transfer steps,

(59) Massi, F.; Grey, M.; Palmer, A. *Protein Sci.* **2005**, *14*, 735–42.
(60) Majumdar, A.; Ghose, R. *J. Biomol. NMR* **2004**, *28*, 213–27.
(61) Dittmer, J.; Bodenhausen, G. *J. Am. Chem. Soc.* **2004**, *126*, 1314–5.
(62) Pervushin, K.; Wider, G.; Wüthrich, K. *J. Biomol. NMR* **1998**, *12*, 345–8.
(63) Cordier, F.; Grzesiek, S. *J. Am. Chem. Soc.* **1999**, *121*, 1601–2.
(64) Lakomek, N.; Fares, C.; Becker, S.; Carlomagno, T.; Meiler, J.; Griesinger, C. *Angew. Chem., Int. Ed.* **2005**, *44*, 7776–8.
(65) Lakomek, N.; Walter, K.; Fares, C.; Lange, O.; de Groot, B.; Grubmuller, H.; Brüschweiler, R.; Munk, A.; Becker, S.; Meiler, J.; Griesinger, C. *J. Biomol. NMR* **2008**, *41*, 139–55.
(66) Mandel, A.; Akke, M.; Palmer, A. *J. Mol. Biol.* **1995**, *246*, 144–63.
(67) Carr, P. A.; Erickson, H. P.; Palmer, A. G. *Structure* **1997**, *5*, 949–59.
(68) Bouvignies, G.; Bernado, P.; Meier, S.; Cho, K.; Grzesiek, S.; Brüschweiler, R.; Blackledge, M. *Proc. Natl. Acad. Sci. U.S.A.* **2005**, *102*, 13885–90.

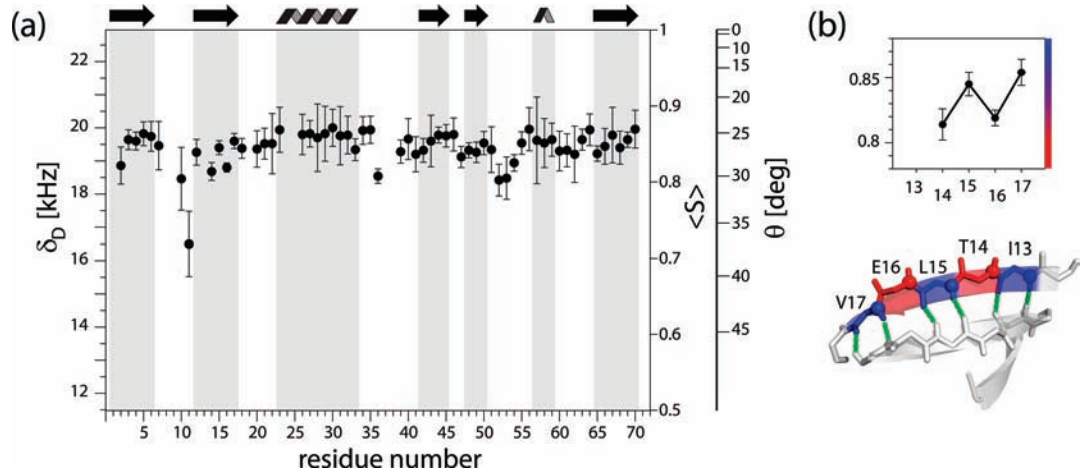

Figure 5. (a) Experimental values of the $^1H-^{15}N$ dipolar coupling δ_D as a function of the residue number in ubiquitin. The order parameter, shown on the right side, is based on an assumed H−N distance of 1.02 Å. The angle θ refers to the cone half-angle if the order parameter is interpreted within the diffusion-in-a-cone model.[51] Error bars were obtained from inspection of $\chi^2_{red.}$ as described in Materials and Methods. (b) Enlargement of the values for residues T14−V17 to illustrate the alternating low and high values of the order parameter S in the β-strand 2, depending on hydrogen bonding and on the orientation of the side chains pointing out or into the hydrophobic core of the protein. Note the complementary alternation of R_1 rates, Figure 6.

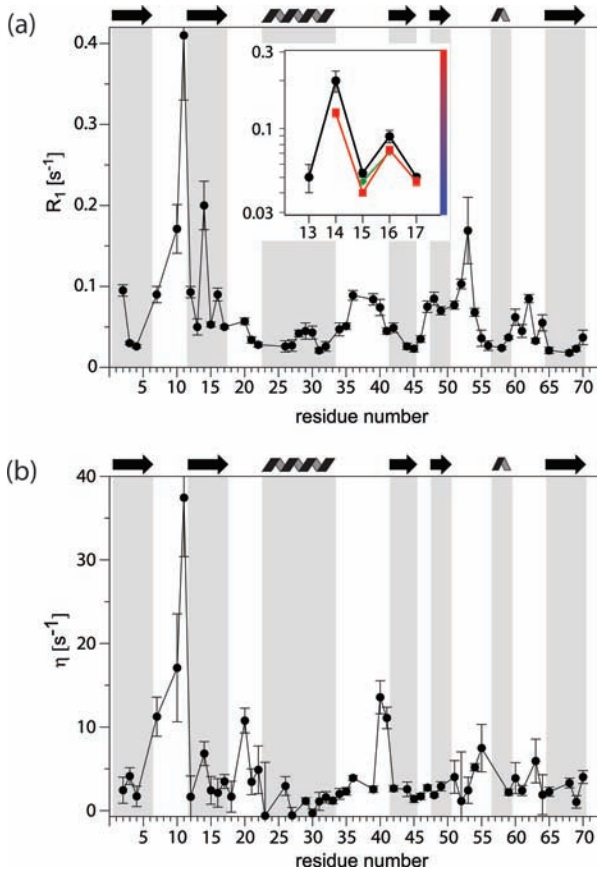

Figure 6. ^{15}N relaxation rate constants measured at 14.09 T as a function of the residue position in the primary sequence of ubiquitin. (a) ^{15}N R_1 relaxation rate constants and (b) ^{15}N CSA, ^1H,^{15}N dipole cross-correlated relaxation-rate constant. The insert in (a) shows R_1 data of the region I13−V17 measured at 11.74 T (green), 14.09 T (black), and 19.96 T (red).

similar to the pulse sequence shown in Figure 1. Through their dependence on the spectral-density function at nonzero frequencies, the relaxation-rate constants depend on the strength of the static magnetic field. We have measured values of R_1 at 11.74, 14.09, and 19.96 T and values of η at 14.09 and 19.96 T. Figure 6 shows residue-resolved relaxation-rate constants measured at 14.09 T. Large relaxation-rate constants (both for R_1 and η) are generally found in loops, while lower values are observed in other secondary-structure elements. The most prominent feature of these data are the relaxation-rate constants in the loop connecting the first two β-strands (T7−K11), where residues with the largest R_1 values and cross-correlated relaxation-rate constants are located. The fast cross-correlated relaxation clearly shows that nanosecond motion is present in this loop. We have already noted that in this region cross-peaks (L8, T9) are unobservable and that the smallest dipolar order parameter is also found for a residue located in this loop (K11). Large R_1 values are also found in the loop regions of residues E34 to Q41 and L50 to L56. In the same regions significant cross-correlated relaxation is detected. Interestingly, and in analogy to a trend observed for dipolar couplings (Figure 5b), an alternating pattern of fast/slow R_1 relaxation is detected in the region from T12 to V17, where amide ^{15}N nuclei of residues with side chains pointing into the hydrophobic core (I13, L15) display significantly slower R_1 relaxation than those in the neighboring residues (T12, T14, and E16) of which the side chains point outward. A similar alternating pattern has been reported from R_1 measurements in a SH3 domain in the solid state.[47]

Model-Free Fit of Dipolar Couplings and Relaxation Data. From the above relaxation and dipolar coupling data, a number of regions with increased flexibility can be identified. Dipolar coupling data (Figure 5) show that increased flexibility, averaged over all relevant time scales, is found in the first loop, the loop following the α-helix, and the loop consisting of residues L50 to T55. In all these regions, the detection of sizable cross-correlated relaxation shows the presence of motion slower than a few nanoseconds (Figure 6b). To obtain quantitative information about the time scale(s) of motion for each residue, dipolar couplings and up to five different relaxation-rate constants (R_1 at three different field strengths, η at two different field strengths) were used in an extended model-free analysis. This approach assumes that there are two different time scales of motion, characterizing fast and slow dynamics, each with its order parameter and its correlation time, according to the spectral density function given in eq 5. In the framework of this model, the experimentally determined, global order parameter obtained

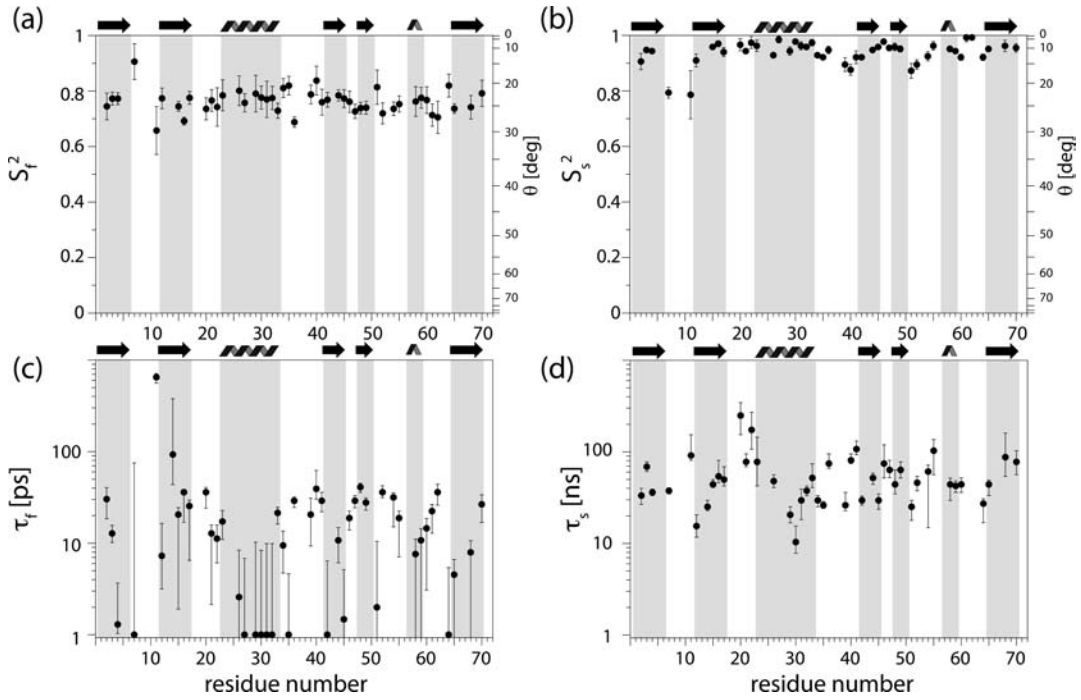

Figure 7. Extended model-free fit results. (a) Squared order parameters for fast (S_f^2) and (b) slow motion (S_s^2) obtained from an extended model-free fit as a function of the primary sequence of ubiquitin. The angle θ refers to the cone opening half-angle if the order parameter is interpreted within the diffusion-in-a-cone model.[51] Correlation time for (c) fast and (d) slow motion. Residues for which less than five experimental observables are available were not analyzed. In addition, fit of the data of residues G10 and T14 resulted in high χ^2 and unphysical fit parameters (see Figure S12). Therefore, these data were omitted. In the cases of the missing residues, qualitative information about the presence of nanosecond motion is nevertheless possible by inspection of the cross-correlated relaxation-rate constants shown in Figure 5b.

from the dipolar couplings is the product of the fast- and the slow-dynamics order parameters; i.e., $S^2 = S_f^2 S_s^2$ because the dipolar couplings are averaged by all processes that are on a time scale shorter than microseconds. Order parameters and correlation times on these two time scales, i.e. four model parameters, were obtained for residues for which at least five experimental observables, i.e., the dipolar coupling and four relaxation-rate constants, were available, thus excluding some residues for which resonance overlap or low sensitivity prohibited extraction of the full data set.

Figure 7 shows order parameters of fast (Figure 7a) and slow (Figure 7b) dynamics obtained from the extended model-free analysis. S_f^2 is in the range 0.7−0.85 (Figure 7a) for the vast majority of residues and appears to be relatively uniform throughout the sequence. Slightly lower order parameters are found for some residues located in loop regions (K11, I36, I61, and Q62). The correlation times corresponding to the fast-dynamics order parameters are in the range of tens of picoseconds (see Figure 7c). This time scale is known to be typical for local bond-vector librations and peptide plane fluctuations. While the fast-motion order parameters are relatively uniform, slow-motion order parameters, shown in Figure 7b, show more variations. For the majority of residues, the order parameter for the slow motion is close to 1. However, three regions with low S_s^2 order parameters can be identified, as expected from the cross-correlated relaxation data. The lowest S_s^2 are obtained for T7 and K11, located at the beginning and at the end of the first loop, respectively. This loop appears as the most dynamic region not only on nanosecond but also on picosecond time scales. As noted above, two residues in this loop are invisible, and the fast transverse dephasing observed for ^{15}N sites in this loop suggests the presence of slow motion. In addition to this region, stretches of consecutive residues with low S_s^2 are found in the loop containing residues E34 to Q41 and in the loop between residues E51 and L56. The correlation time corresponding to these residues, τ_s, is in the range 25−100 ns. This time scale is in agreement with the general picture of loop reorientation motions.[69] It is interesting to note that also most residues located in secondary structure elements appear to have small-amplitude nanosecond dynamics with order parameters S_s^2 in the range 0.95−0.97 for most residues and corresponding correlation times on the order of tens of nanoseconds. If the order parameter is interpreted in terms of the diffusion-in-a-cone model, this corresponds to a cone opening half-angle of <10°. The presence of (at least small-amplitude) nanosecond dynamics at many backbone sites is directly evidenced by the observation of cross-correlated relaxation-rate constants exceeding several s^{-1}, especially in the measurements at 19.96 T (see Table S3 of the Supporting Information). Cross-correlated relaxation-rate constants of this magnitude can only be expected when the time scale of motion exceeds several nanoseconds (see Figure S9).

We have also considered a fit to a simpler model that uses only two parameters (one order parameter and one correlation time) instead of four. Table S5 of the Supporting Information reports the fitted parameters from this simpler approach. However, the use of the more complex model can be justified for most residues, as follows. For all residues where six experimental parameters were available—allowing the calculation of a reduced χ^2 for the four-parameter model—the reduced χ^2 of the more complex four-parameter model was substantially reduced, on average reduced by 1 order of magnitude, upon increasing the number of fit parameters. For a more quantitative measure of the validity of the more complex extended model-free approach we turned to *F*-test analysis (see Table S6). For

(69) Henzler-Wildman, K.; Kern, D. *Nature* **2007**, *450*, 964–72.

the majority of residues (18 out of 27) where six experimental data are available, the *F*-test reveals that the extended model-free fit is explaining the data significantly better the simple model-free (using the canonical cutoff of 0.05 for the *p* value). There are also 10 residues where six experimental observables are available, but for which the extended model-free treatment is rejected by the p value < 0.05 criterion. The *p* value in these cases lies between 0.06 and 0.18 (residues Q2, G10, L15, I30, D32, Q49, D52, T55, and N60). For residues where only four relaxation rates are available (primarily because of resonance overlap at the lowest available field strength) the extended model is accepted only in four cases (residues F4, V17, K29, and F45), while in 12 cases the four-parameter model, fit to only five data points, is rejected by the *F*-test (K11, T12, T22, I23, Q31, K33, D39, E51, E58, Q62, G64, and H68). While it is evident that the extended model-free approach is at the limit of feasibility even with a very comprehensive set of data as used in this study, the *F*-test confirms its validity in most cases where sufficient data are available, and the use of the extended version is encouraged especially for those residues where cross-correlated relaxation reveals slow dynamics. We note that in cases where the amplitude of the nanosecond dynamics is very small resulting in slow-motion order parameter S_s^2 close to 1, the application of the more complex model does not significantly alter the fast-motion order parameter, due to the simple relation between the dipolar order parameter (S^2) and the two model-free order parameters ($S^2 = S_s^2 S_f^2$). The conclusions we make on fast dynamics are, therefore, not significantly dependent on the choice of model.

The obtained parameters of the model-free analysis can also be used to back-calculate transverse relaxation-rate constants. The experimentally determined R_2' values can only provide an upper bound for R_2 rate constants because of contributions from coherent mechanisms to R_2' in solids. As expected, all experimental R_2' rate constants exceed the calculated ones (see Figure S14 of the Supporting Information), and we, thus, note that our model-free parameters are in agreement with transverse relaxation data.

Conclusions

In summary, we have presented a detailed and comprehensive investigation of protein backbone dynamics in ubiquitin in the solid state based on proton-detected solid-state NMR experiments using highly deuterated samples and a large set of proton-detected scalar-coupling-based experiments. The experimental approach for the measurement of dipolar-coupling-based order parameters using REDOR experiments is remarkably robust with respect to experimental imperfections and is expected to prove useful for the study of other precipitated proteins, amyloid fibrils, or membrane proteins. From an experimental point of view, it should be noted that such a solid-state NMR study can be performed on a single sample of only several milligrams (<10 mg) of protein, giving insight into dynamics over many time scales. We further expect that the REDOR approach will also be of great use for other sites in proteins. For example, the REDOR experiment applied to specifically protonated methyl groups in an otherwise deuterated environment will provide valuable insight into the motional amplitudes of side chains. It will also be of interest to better define backbone mobility by a combination of different dipolar couplings measured along the backbone. For example, N−C couplings, measured with REDOR or TEDOR[70] experiments, can be a promising complement to the H−N couplings measured here and can be expected to reveal anisotropy of backbone motion over time scales up to microseconds.

Our study confirms that sizable dynamics are present in ubiquitin even in crystalline form. We find direct evidence of nanosecond motion in the backbone, primarily in three loop regions, as revealed by cross-correlated relaxation. The observation of very different behavior for different regions in the protein, with some residues in flexible regions even broadened beyond detection, rules out the possibility that concerted overall motion of the molecule in the crystal, such as overall rocking, is the predominant mechanism of relaxation in the solid state.

With the availability of robust approaches for quantifying protein dynamics in the solid state it will also be of considerable interest to determine differences in dynamics between solid- and solution-state samples, a subject that has seen some attention recently.[71,72] Ongoing research is directed toward such a description of the impact of the crystalline environment on protein backbone and side-chain dynamics. These data will also provide the basis for understanding the dynamics of systems where intermolecular contacts are an inherent feature, such as amyloid fibrils.

Materials and Methods

Sample Preparation. Uniformly ^2H,^{13}C,^{15}N-labeled ubiquitin was produced by overexpression in *Escherichia coli* BL21 in M9 minimal medium, containing 2 g/L ^2H,^{13}C glucose as the sole carbon source and 1 g/L $^{15}N^2H_4$. To minimize contamination from ^1H, all components of the buffers were first dissolved in D_2O and lyophilized prior to the preparation of the buffers. Standard purification steps were performed in H_2O-based buffer solutions. The protein was crystallized using 2-methylpentane-2,4-diol-d_{12} (Sigma-Aldrich), as described previously.[55] The crystallization buffer contained a H_2O/D_2O mixture resulting in incorporation of ^1H (^2H) at exchangeable protein sites to 30% (70%). Crystals were grown for 2−3 weeks and filled into a 1.8 or a 1.3 mm rotor using an ultracentrifuge device.[73] In the process of filling the rotors, 3−4 μL of a 100 mM solution of sodium 3-(trimethylsilyl)-1-propanesulfonic acid (DSS) was added to the suspension of crystals, for chemical-shift referencing. The volume of the 1.8 mm rotor used for the REDOR experiments was restricted to about 40% of its original volume using Teflon spacers to increase the homogeneity of the B_1 field over the sample volume. This restriction was done for an ongoing comparison to other recoupling sequences where rf-field homogeneity is more crucial, and we note that due to the robustness of the REDOR experiment with respect to B_1 inhomogeneity, this volume restriction would not be necessary in general. The two different rotors used in this study all stem from the same protein production and crystallization batch, in order to ensure maximum possible comparability between samples used at different field strengths.

NMR Spectroscopy. NMR experiments were performed on a Varian Infinity+ 500 spectrometer, operating at a static magnetic field strength of 11.74 T, a Bruker Avance 600 spectrometer, operating at 14.09 T, and a Bruker Avance 850 spectrometer, operating at 19.96 T. A custom-made 1.8 mm double-resonance probe and a 1.8 mm triple-resonance probe (Ago Samoson, Tallinn,

(70) Jaroniec, C.; Filip, C.; Griffin, R. *J. Am. Chem. Soc.* **2002**, *124*, 10728–42.
(71) Chevelkov, V.; Xue, Y.; Linser, R.; Skrynnikov, N. R.; Reif, B. *J. Am. Chem. Soc.* **2010**, *132*, 5015–7.
(72) Agarwal, V.; Xue, Y.; Reif, B.; Skrynnikov, N. *J. Am. Chem. Soc.* **2008**, *130*, 16611–21.
(73) Böckmann, A.; Gardiennet, C.; Verel, R.; Hunkeler, A.; Loquet, A.; Pintacuda, G.; Emsley, L.; Meier, B.; Lesage, A. *J. Biomol. NMR* **2009**, *45*, 319–27.

Estonia) were used for measurements at 11.74 and 14.09 T, respectively, while a commercial 1.3 mm probe (Bruker Biospin, Karlsruhe, Germany) was used for measurements at 19.96 T. The MAS frequency was set to 45 kHz for all relaxation measurements and to 40 kHz for the REDOR experiments performed at 14.09 T. The effective sample temperature was set to 301 K, using the chemical shift of the bulk-water line as an internal temperature reference.

Assignment of the amide H−N correlation peaks was obtained from a series of *J*-based 3D correlation spectra (HNCO, HNCA, and HN(CO)CA) similar to experiments described previously,[54] and ^{13}C,^{15}N resonance frequencies closely match previously reported assignments.[55,56]

^{15}N R_1 relaxation-rate constants were measured with the pulse sequence shown in Figure S6a of the Supporting Information. Water suppression was achieved using a 20 ms long saturation pulse, while magnetization was stored on ^{15}N. Twelve (at 11.74 T), nine (14.09 T) and ten (19.96 T) spectra were recorded with different lengths of the relaxation delay, and the maximum delays were 25, 25, and 40 s, respectively. Cross-correlated relaxation-rate constants were obtained using the pulse scheme of Figure S6b in the Supporting Information. Nine (nineteen) delays were sampled on the decay curves with a maximum value of 120 (140) ms in experiments performed at 14.09 T (19.96 T). Examples of decay curves are shown as Supporting Information

REDOR experiments were recorded with the pulse sequence of Figure 1 at 14.09 T. Delay settings and pulse phases are noted in the figure caption except for the delay τ. Three independent experimental series were measured. In two of these series (shown in Figure 3), the delay τ between the start of the rotor period and the subsequent ^{1}H π pulse was set to 2.5 and 3.5 μs (applying the ^{1}H π pulses for 4 μs; i.e., the delay between consecutive pulses was 0.5 and 1 μs, respectively), while in the third experimental series τ was set to 3 μs and the ^{1}H π pulses of the REDOR pulse train were applied at a field strength of 100 kHz (5 μs pulses). The different choice of τ and of the pulse length leads to a different frequency of the dephasing. All ^{15}N π pulses, including the central pulse of the REDOR block, were applied at a field strength of 50 kHz (10 μs pulse length). Suppression of the unwanted solvent signal was achieved by a saturation pulse of 5 ms duration, as proposed previously.[74] Reference experiments were obtained by omitting the ^{1}H π pulses during the REDOR period. Reference intensities in the spectra at different dephasing times were almost identical within error bars, which is explained by the slow ^{15}N transverse dephasing.[75] Therefore, only six reference spectra were recorded, and reference intensities $S_0(\tau_{mix})$ for each point on the REDOR curve were obtained by linearly interpolating between the available reference spectra. Within the specified error margins, identical results would be obtained by omitting the linear interpolation and taking a single reference intensity for all points on the REDOR curve. Each 2D experiment was recorded for approximately 2 h.

All spectra were processed using the nmrPipe software[76] and analyzed with the nmrView software (OneMoon Scientific Inc.). Processing involved apodization with a sine-squared function, shifted by 0.45π and baseline correction.

Numerical Simulations and Extraction of Dipolar Couplings. Theoretical REDOR curves were simulated numerically using the software package GAMMA.[77] A series of simulations was performed assuming a two-spin ^{1}H−^{15}N system and varying the anisotropy of δ_D in the range from 1 to 24 kHz in steps of 20 Hz. The obtained dephasing curves were used to fit the experimental data (see below). In all simulations the chemical-shift tensors of ^{15}N and ^{1}H were assumed to be axially symmetric with values of the reduced anisotropy $\Delta\sigma = \sigma_{zz} - \sigma_{xx}$ of −170 and +9 ppm, respectively. Note that the CSA parameters have essentially no influence on the dephasing (see Figures S1 and S2).

The anisotropy of the ^{1}H−^{15}N dipolar-coupling tensors in ubiquitin was obtained by comparing the points on the experimental REDOR curves, $(S(\tau_{mix}) - S_0(\tau_{mix}))/S_0(\tau_{mix})$, with those from the numerical two-spin simulations. The best-fit value of δ_D was found by minimizing the reduced χ^2 (χ^2_{red}) for the three data sets simultaneously, i.e., by searching the minimum of the target function

$$\chi^2_{red} = \frac{1}{3}\sum_{i=1}^{3}\frac{1}{N_i - p - 1}\sum_{1}^{N}\frac{((\Delta S(\tau)/S_0(\tau))_{i,expt} - (\Delta S(\tau)/S_0(\tau))_{i,calc})^2}{\sigma_{i,expt}{}^2} \quad (6)$$

Here, N_i is the number of REDOR data points in the ith experimental series, $\Delta S(\tau_{mix})/S_0(\tau_{mix})$, which were 31, 29, and 29, respectively, in the three independent measurement series. The only free parameter is the value of δ_D, thus $p = 1$. σ_{expt} is the experimental error associated with a given value of $\Delta S(\tau_{mix})/S_0(\tau_{mix})$. This error was estimated from two times the standard deviation of the spectral noise level. Error margins of the fit parameter δ_D were estimated by inspecting the χ^2_{red} profile. Reported error bars correspond to the value of δ_D where χ^2_{red} exceeds its minimum value by 1. It should be noted that each individual data set out of the three data sets measured here would suffice to obtain the dipolar coupling. Recording more than one series effectively increases the precision with which δ_D is extracted. The values of δ_D derived from fits to the individual series agree with the value obtained from simultaneous fit to the three series within the error of the overall fit.

Relaxation Data Fitting. ^{15}N R_1 relaxation-rate constants were obtained by fitting the experimentally observed peak heights to two-parameter monoexponential functions. Similarly, to obtain cross-correlated relaxation-rate constants, the upfield and downfield components observed in in-phase anti-phase (IPAP)-edited experiments were fit separately using two-parameter monoexponential functions. Cross-correlated relaxation-rate constants, η, were calculated from the apparent transverse relaxation-rate constants of the downfield and upfield components, $R_2{}^\alpha$ and $R_2{}^\beta$, as $\eta = 0.5(R_2{}^\alpha - R_2{}^\beta)$. The details of the measurement and analysis of cross-correlated relaxation have been discussed by Chevelkov et al.[49] and Skrynnikov.[50] Error bars of relaxation-rate constants were obtained from 500 Monte Carlo runs, based on twice the spectral noise level.

We have also considered the potential effect that hydrogen/deuterium exchange could have on the measured longitudinal relaxation rates by comparing R_1 data with exchange-rate constants obtained from solution-state exchange measurements, corrected for the pH used in this study.[78,79] Generally, exchange-rate constants, as obtained from solution-state data, are about 1 order of magnitude lower than observed relaxation rates (for secondary structure elements even more), meaning that exchange of amide protons during the relaxation measurements is negligible. One notable exception is A46, for which the calculated exchange rate constant (obtained from solution data) is larger than the experimentally observed relaxation rate.

Model-Free Analysis. The ^{1}H−^{15}N dipolar coupling, which directly defines the overall order parameter $S^2 = S_s{}^2 S_f{}^2$, and up to five relaxation-rate constants were used to fit an extended model-

(74) Zhou, D.; Rienstra, C. *J. Magn. Reson.* **2008**, *192*, 167–72.
(75) Schanda, P.; Huber, M.; Verel, R.; Ernst, M.; Meier, B. *Angew. Chem., Int. Ed.* **2009**, *48*, 9322–5.
(76) Delaglio, F.; Grzesiek, S.; Vuister, G.; Zhu, G.; Pfeifer, J.; Bax, A. *J. Biomol. NMR* **1995**, *6*, 277–93.
(77) Smith, S.; Levante, T.; Meier, B.; Ernst, R. *J. Magn. Reson. A* **1994**, *106*, 75–105.
(78) Bougault, C.; Feng, L. M.; Glushka, J.; Kupce, E.; Prestegard, J. H. *J. Biomol. NMR* **2004**, *28*, 385–90.
(79) Cordier, F.; Grzesiek, S. *J. Mol. Biol.* **2002**, *317*, 739–52.
(80) Chekmenev, E.; Zhang, Q.; Waddell, K.; Mashuta, M.; Wittebort, R. *J. Am. Chem. Soc.* **2004**, *126*, 379–84.

free spectral-density function, given by eq 5. In all analyses, the H−N bond length was set to 1.02 Å and the ^{15}N CSA tensor was assumed to be axially symmetric with a value of $\Delta\sigma = -170$ ppm[80]. Data fitting was performed using a multidimensional grid search minimizing the χ^2 function, defined as

$$\chi^2 = \sum_i \frac{(\Gamma_i^{\text{expt}} - \Gamma_i^{\text{calc}})^2}{\sigma_i^2} \tag{7}$$

where Γ_i^{expt} (Γ_i^{calc}) is the ith relaxation-rate constant obtained from experiment (from calculation) with an experimental uncertainty σ_i. Ranging from 0.4 to 1 for S_f^2 and S_s^2, from 10^{-12} to 5×10^{-9} s for τ_f, and from 10^{-9} to $10^{-4.5}$ s for τ_s, 160 grid points were used in each dimension. The sampling on this grid was linear for the order parameters and logarithmic for the correlation times. For residues where six data points are available, it is possible to calculate a reduced χ^2 defined as

$$\chi^2_{\text{red}} = \frac{1}{N - p - 1} \sum_i \frac{(\Gamma_i^{\text{expt}} - \Gamma_i^{\text{calc}})^2}{\sigma_i^2} \tag{8}$$

where N is the number of experimental data points (6) and p is the number of fit parameters (4). (For residues where less than six experimental observables were available, χ^2_{red} is infinite.)

The two-parameter model-free analysis was performed using the spectral density function

$$J(\omega) = (1 - S^2)\frac{\tau}{1 + (\omega\tau)^2} \tag{9}$$

To estimate the error margins of all fit parameters, Monte Carlo simulations were performed. By adding Gaussian noise to the back-calculated values of δ_D, R_1, and η that were obtained from the best extended model-free fit to the experimental relaxation rates and dipolar couplings, 200 synthetic data sets were generated. Model-free parameters were obtained for each individual "noisy" data set, and the standard deviation of the 200 fit parameters is used as an estimate for the uncertainty of the fit parameters. A discussion of the error margins of fast motion is presented in the Supporting Information (Figure S13).

The analysis of all data was based on the assumption that the rigid-limit H−N bond length is 1.02 Å.[43] A value of 1.015 Å has also been proposed previously.[42] Accurate measurement of this equilibrium bond length is complicated by the fact that changes in bond length and the presence of dynamics are experimentally difficult to disentangle. To assess the effect of a different rigid-limit bond length on our analysis, we performed all data fitting also with $r_{NH} = 1.015$ Å. This leads to slightly lower values of the dipolar-coupling-derived order parameter on the basis of eq 2. It is interesting to note, however, that S_s^2 is essentially unchanged in such a data analysis and that the difference in the bond length exclusively translates to somewhat smaller S_f^2 on average by $\Delta S_f^2 = 0.02$, as well as some minor changes in the correlation times (see Figure S10 of the Supporting Information). This reflects the fact that the determination of S_f^2 critically relies on the availability of a dipolar-coupling-derived S^2, a view that is also supported from inspection of the Monte Carlo analysis of the model-free fit (see Figure S11 of the Supporting Information). We note from this analysis that the possible systematic errors from uncertainties in the value of the rigid-limit bond length are not important in the present context.

Finally, we note that a slightly different form of the extended model-free approach has been used in a recent joint analysis of solid- and solution-state data.[27] This modified version was initially designed to provide a better separation between slow internal motion and overall tumbling in solution.[81] In the absence of overall tumbling, i.e., when treating solid-state data, this is, however, not an issue, and we, thus, use the original formulation of the extended model-free approach.[53]

Acknowledgment. This work was supported by the Swiss National Science Foundation and the ETH. P.S. acknowledges a postdoctoral fellowship from the ETH. Dr. René Verel is acknowledged for insightful discussions.

Supporting Information Available: Text describing numerical simulations of the REDOR experiment investigating the robustness of the experiment, figures showing the effect of rf-field inhomogeneity, isotropic chemical-shift offsets, variations of the anisotropic chemical shift, and the influence of a third spin on the REDOR decoupling, pulse schemes for the measurement of ^{15}N R_1 and ^{15}N-CSA, ^{1}H,^{15}N-dipole cross-correlated relaxation, experimental examples of relaxation decay profiles, calculated values of the two relaxation rate constants, R_1 and η, as a function of model-free parameters at two different magnetic field strengths, used to illustrate the dependence of these rates on dynamics, comparison of model-free order parameters obtained from an analysis that assumes H−N bond lengths of 1.015 and of 1.02 Å, correlation of S^2 and S_f^2 values obtained in the Monte Carlo analysis of an example residue, residue-wise transverse dephasing rate constants, R_2', correlation of dipolar couplings to $^1H^N$ chemical shifts, examples of χ^2_{red} surfaces of the model-free grid search, and tables giving chemical shift assignments, all experimental data, and fit results of the two-parameter and four-parameter model-free fits including statistical analysis. This material is available free of charge via the Internet at http://pubs.acs.org.

JA100726A

(81) Skrynnikov, N.; Millet, O.; Kay, L. *J. Am. Chem. Soc.* **2002**, *124*, 6449–60.